©1999 The Visualization Society of Japan and Ohmsha, Ltd.
Journal of Visualization, Vol. 2, No. 2 (1999) 127-134

# 3D Simulation and Visualization of Unsteady Wake Flow behind a Cylinder

Osawa, Y.* and Tezduyar, T.*

* Mechanical Engineering and Materials Science, Army HPC Research Center, Rice University - MS 321, 6100 Main Street, Houston, TX 77005, USA.

Received 6 April 1999.
Revised 2 July 1999.

***Abstract*:** In this paper we focus on 3D simulation of unsteady wake flow behind a circular cylinder. We show that in addition to accurate formulations and sufficiently-refined meshes, efficient computing methods are essential components of an effective simulation strategy. We use the Multi-Domain Method (MDM) we developed recently in computation of two cases. At Reynolds number 300, we demonstrate how the MDM enables us to use highly-refined meshes to capture wake patterns which we otherwise cannot fully represent. At Reynolds number 140, we show that with the MDM we can extend our computations sufficiently downstream, and with sufficient accuracy, to successfully capture the second phase of the Karman vortex street, which has been observed in laboratory experiments, and which has double the spacing between the vortices compared to the first phase.

***Keywords*:** unsteady wake flow, multi-domain method, vortex shedding.

## 1. Introduction:

Simulation and visualization of unsteady wake flow behind a circular cylinder has attracted a large number of computational researchers by providing a platform for testing new computational ideas, comparing with experimental results, and better understanding some of the fundamental fluid mechanics issues involved. The large majority of the work of the past has been limited to 2D simulations where it is possible to use very, very refined meshes. 3D simulations are more challenging because using highly-refined meshes to capture 3D behavior could increase the computational burden significantly, especially if one wishes to extend the computations sufficiently downstream, and with sufficient accuracy, to successfully capture a behavior expected to be seen far downstream, such as 300 diameters away.

Many researchers reported computational and experimental studies of 3D behavior behind a circular cylinder (see for example [1-6]). The unsteady behavior at far downstream, including the second phase of the Karman vortex shedding, was particularly emphasized first in [1], followed by [2-4].

In this paper we present 3D simulation and visualization of two cases of unsteady wake flow behind a cylinder. In the first case the Reynolds is 300, and the purpose is to see how using highly-refined meshes enables the detailed capture of 3D effects and vortex shedding in the wake as far as 30 diameters ($\overline{d}$) downstream. In the second case the Reynolds number is 140. The second phase of the Karman vortex shedding at this Reynolds number was reported earlier, and Cimbala [3] attributes this behavior to hydrodynamic instability. Williamson [5], on the other hand, suggests that this behavior is caused by the sensitivity of the wake to small-scale perturbations. Our purpose here was to capture the wake as far as $300\overline{d}$ downstream, investigate the formation of the second phase of the vortex shedding, and see how the 2D and 3D approaches differ in successful capture of this second phase.

To be able to carry out these simulations with sufficient mesh resolution and with sufficiently long computational domains, we need efficient computing methods which will enable us to accomplish this goal without exceeding the practical limits of our computational resources. The Multi-Domain Method (MDM) [7,8] developed recently was originally intended for parallel 3D computation of the unsteady wake flow in the far downstream of an object and the influence of this wake on secondary objects located far downstream. Also recently, a computational technique [9] largely based on the MDM was designed for simulation of unsteady wake flows behind a circular cylinder, including cases with computational domains extending far downstream.

The core flow solution technique in the MDM is a stabilized finite formulation of the Navier-Stokes equations of incompressible flows (see [7,8]). The stabilization techniques are the streamline-upwind/Petrov-Galerkin (SUPG) [10] and pressure-stabilizing/Petrov-Galerkin (PSPG) [11] stabilizations. With these stabilization techniques, we maintain the stability of the numerical formulation without introducing excessive numerical dissipation. In the MDM, the computational domain is divided into an ordered sequence of overlapping subdomains, where the cylinder is placed in the first subdomain. Each subsequent subdomain receives its inflow boundary conditions from the subdomain preceding it. This strategy allows us to divide the computational task into manageable pieces and carry out the computations for different subdomains essentially in parallel. This parallelism is in addition to the main parallelism we have within individual subdomains. The core flow solver and the MDM have been implemented on parallel computing platforms such as the CRAY T3E-900 and T3E-1200, and this further increases the speed of the computations.

In Section 2 we provide an overview of the MDM. The numerical results from the first (at *Re*=300) and second (at *Re*=140) simulation cases are presented in Section 3 and Section 4, respectively. We provide our brief concluding remarks in Section 5.

## 2. The Multi-Domain Method for Wake Computations

In the MDM, the computational domain is divided into an ordered sequence of overlapping subdomains. Subdomain-1 (SD-1) contains the cylinder and is used for computation of the unsteady flow around and in the near wake. The inflow boundary conditions for this first subdomain are the free-stream conditions. This subdomain is discretized with an unstructured mesh, and the computations are carried out by using a general-purpose implementation of the finite element formulation, applicable to elements of any shape. In this subdomain, somewhere sufficiently ahead of the outflow boundary, we place an "outflow layer." As the computations proceed, the inflow boundary conditions for the subsequent subdomain are extracted from this outflow layer.

The subsequent subdomains, SD-2, SD-3, ..., are used for computation of the unsteady flow in wake regions further downstream. Typically these subdomains are longer than SD-1, but have mesh resolutions comparable to that of SD-1, and therefore lead to much larger equation systems to be solved. However, these subdomains do not contain any objects, and therefore are discretized with highly-refined meshes with very regular-shaped elements. Because the element shapes are special, the computations are carried out with a special-purpose implementation of the finite element formulation. In this special implementation, the simplified data structure is recognized and exploited to speed up the computation. The special-purpose implementation includes performing the element level integrations analytically rather than numerically. This special-purpose implementation, with proper optimization, yields much higher computational speeds compared to the general-purpose implementation. We note that the computations over SD-2, SD-3, ..., can also be accomplished by methods which might be preferable to the finite element method when meshes with regular-shaped elements are used. The inflow boundary conditions for each of these subdomains are extracted from the outflow layer of the preceding subdomain. The extraction is accomplished by performing a projection operation at each time step. This projection step has also been implemented in parallel.

The computations within each subdomain is carried out in parallel, where the elements in a subdomain are distributed among the available processors in an optimal fashion. Normally we first carry out the computations for SD-1, followed by the computations for SD-2, and so on. However, we note that the computations over these different subdomains can be performed essentially in parallel, provided a leading subdomain is at least one time step ahead of the following subdomain. In fact computations over different subdomains can even be carried out on different computational platforms (essentially) in parallel, because the data transfer between the different platforms would just be a 2D data exchange and therefore would not add a significant communication cost. For further details on the MDM see [8].

## 3. *Re*=300: Effect of Mesh Refinement

The purpose here is to see how using highly-refined meshes in simulations based on the MDM enables the detailed capture of the 3D effects and vortex shedding. We compare the solutions obtained with the single-domain and multi-domain methods, where the mesh used with the MDM is more refined.

In the single-domain computation, we use the same mesh as the one reported in [6]. The span length of the cylinder is $4\overline{d}$. The upstream, downstream, and crossflow (i.e. top and bottom lateral) boundaries are located, respectively, at $7.5\overline{d}$, $30\overline{d}$, and $7.5\overline{d}$. The mesh consists of 197,948 nodes and 186,240 hexahedral elements, and leads to 760,107 equations. The boundary conditions consist of uniform inflow velocity, zero shear stress and normal velocity at lateral boundaries, traction-free condition at the outflow boundary, and no-slip condition on the cylinder surface. The "outflow layer" is located at $2\overline{d}$ downstream from the cylinder center.

In the multi-domain computation, SD-1 consists of the domain we used in the single-domain computation. The wake subdomain, SD-2, extends $28\overline{d}$, $4\overline{d}$ and $15\overline{d}$ along the streamwise, spanwise, and crossflow directions, respectively. SD-2 mesh consists of 1,163,565 nodes and 1,126,400 hexahedral elements, and leads to 4,553,457 equations. Compared to the wake region of the single-domain model, the number of elements in SD-2 is precisely 2.0 times larger in the spanwise direction, and approximately 3.3 and 1.8 times larger in the streamwise and crossflow directions. The inflow boundary conditions are extracted by projection from the solution obtained in the single-domain computation. The conditions imposed at the lateral and downstream boundaries are the same as those we had in the single-domain model.

The computations were carried out on a CRAY T3E-900. The visualizations were obtained by using an SGI Onyx2 and the visualization software Ensight. Figure 1 shows the isosurfaces corresponding to the 0.5 value of the vorticity magnitude. Figure 1 also shows the in-plane mesh. Clearly the solution over SD-2 captures the flow features in greater detail, and maintains these features all the way to the outflow boundary. In the near wake, the isosurfaces representing the spanwise vorticity of the Karman vortex street are almost straight in the vertical direction. The isosurfaces representing the in-plane vorticity, on the other hand, form horizontally layered arch shapes. These two types of vortices interact with each other as it is revealed by the visualization provided in Fig. 1.

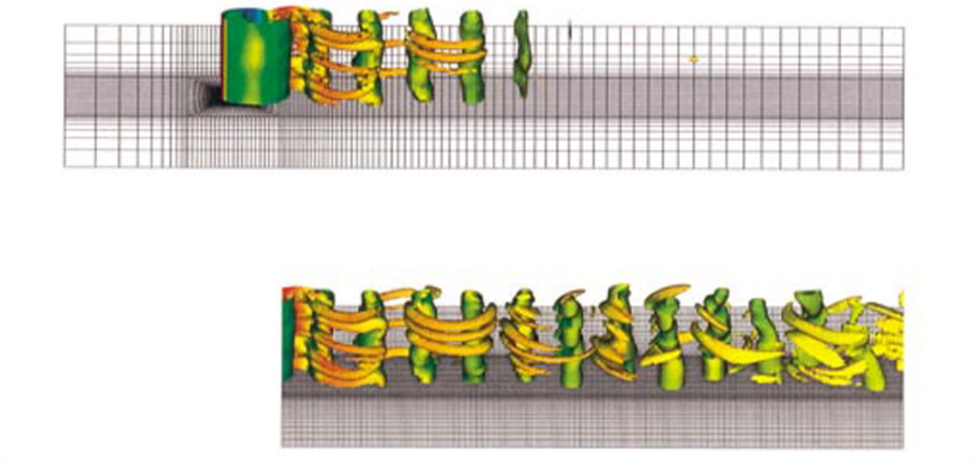

Fig. 1. *Re*=300: effect of mesh refinement. The isosurfaces corresponding to the 0.5 value of the vorticity magnitude. Obtained with the single-domain (upper) and multi-domain (lower) computations.

## 4. *Re*=140

The purpose in this case is to extend our computations sufficiently downstream to capture the long-wake flow behavior including the second phase of the Karman vortex shedding, and to see the difference between attempting this in 2D and 3D.

In the 2D simulation the entire domain is divided into two subdomains (see Fig. 2). For SD-1, the upstream, downstream, and crossflow boundaries are located, respectively, at $7.5\overline{d}$, $30\overline{d}$ and $10\overline{d}$ from the center of the cylinder. SD-1 mesh consists of 8,216 nodes and 8,000 quadrilateral elements, and leads to 24,094 equations. The boundary conditions are imposed in the same way as we did for SD-1 in the *Re*=300 case. The outflow layer is also selected in the same way as before. SD-2 starts at $2\overline{d}$ downstream from the center of the cylinder and extends to $300\overline{d}$. SD-2 mesh consists of 912,033 nodes and 905,920 quadrilateral elements, and leads to 2,723,416 equations. The inflow boundary conditions are extracted by projection from the solution obtained over SD-1. The conditions imposed at the lateral and downstream boundaries are the same as those used for SD-1.

The computations were carried out on a CRAY T3E-1200. Figure 3 shows the vorticity. Figure 4 shows the side view of the elevation plot for the vorticity for SD-2. The color indicates the value of the vorticity. We note that, because of the highly-refined mesh, the near-wake Karman vortices obtained with the SD-2 are more clearly defined. However, we also note that no second phase of vortex shedding is seen in the far wake. A clearly periodic vorticity distribution is observed in the near wake, but this distribution decays downstream (see Fig. 4). According to the laboratory experiments [2,3], the transition between the first and second phases of the vortex shedding is expected at $100\overline{d}$-$150\overline{d}$. However in this 2D simulation, vorticity decays in that region (see Fig. 4). This leads us to

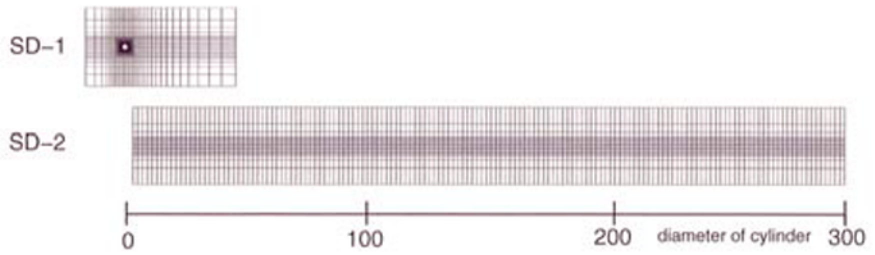

Fig. 2. 2D computation at *Re*=140. Arrangement of the two subdomains. Frames do not show the actual meshes.

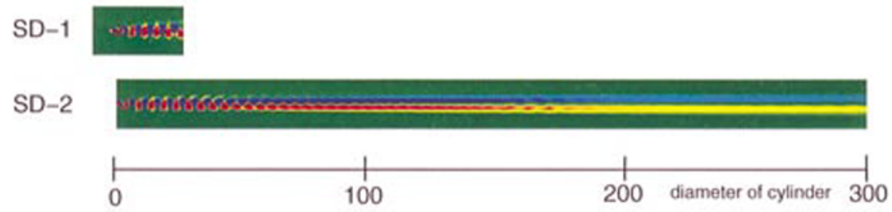

Fig. 3. 2D computation at *Re*=140. Vorticity for SD-1 (upper) and SD-2 (lower).

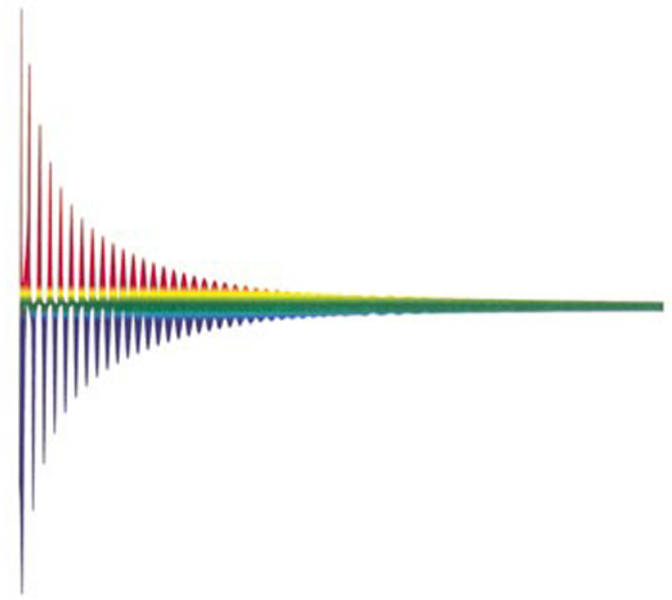

Fig. 4. 2D computation at *Re*=140. Side view of the elevation plot for the vorticity for SD-2. The color indicates the value of the vorticity (red: positive, blue: negative).

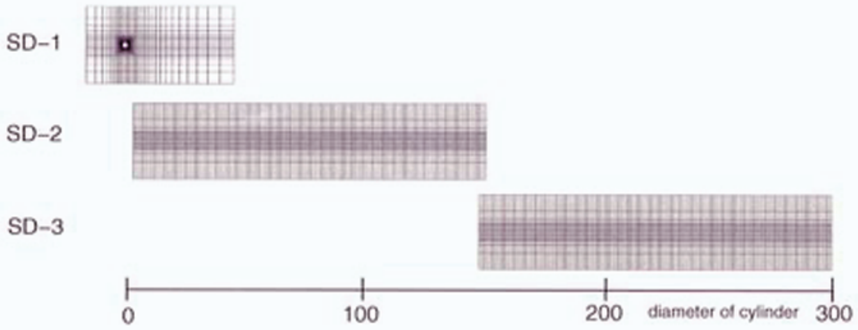

Fig. 5. 3D computation at *Re*=140. Arrangement of the three subdomains. Frames do not show the actual meshes.

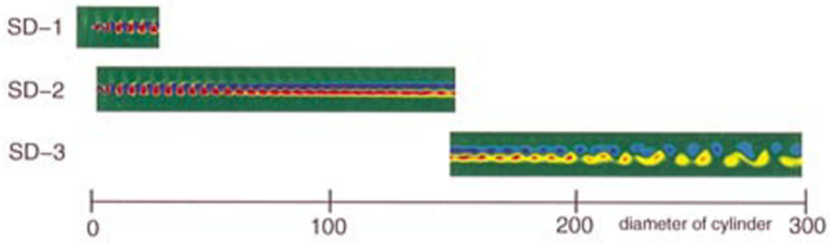

Fig. 6. 3D computation at *Re*=140. Spanwise component of the vorticity for SD-1 (upper), SD-2 (middle), and SD-3 (lower).

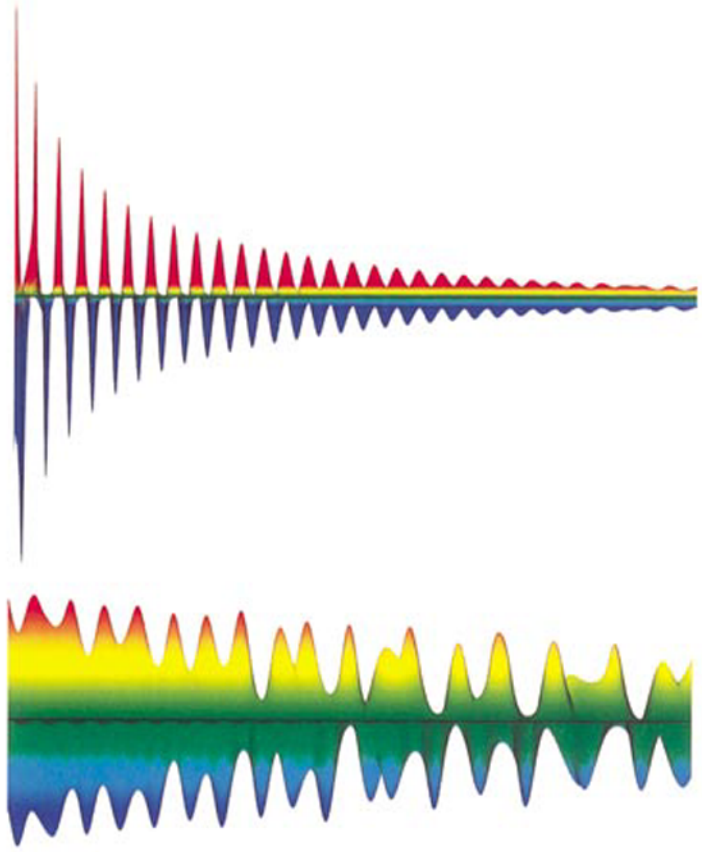

Fig. 7. 3D computation at *Re*=140. Side view of the elevation plot for the spanwise component of the vorticity at the centered horizontal plane for SD-2 (upper) and SD-3 (with different scale) (lower). The color indicates the value of the vorticity (red: positive, blue: negative).

believe that the 3D effects are the cause of the second phase of the vortex shedding.

In 3D simulation the domain is divided into three subdomains (see Fig. 5). The in-plane dimensions of SD-1 are the same as those of SD-1 in 2D simulation. In the spanwise direction, the cylinder and domain dimensions are $4\overline{d}$. The mesh consists of 213,856 nodes and 201,600 hexahedral elements, and leads to 822,479 equations. The boundary conditions are imposed in the same way as we did for earlier SD-1 computations reported in this paper. The outflow layer is also selected in the same way as before. SD-2 starts at $2\overline{d}$ downstream from the center of the cylinder and extends to $155\overline{d}$. SD-3 starts at $150\overline{d}$ and extends to $300\overline{d}$. SD-2 mesh consists of 4,470,025 nodes and 4,308,480 hexahedral elements, and leads to 17,536,577 equations. The inflow boundary conditions are extracted by projection from the solution obtained over SD-1. The conditions imposed at the lateral and downstream boundaries are the same as those used for SD-1. The outflow layer is located at $150\overline{d}$ downstream from the center of the cylinder (i.e. $5\overline{d}$ ahead of the outflow boundary). The mesh density for SD-3 is the same as that for SD-2. SD-3 mesh consists of 4,382,449 nodes and 4,224,000 hexahedral elements, and leads to 17,192,513 equations. The inflow boundary conditions are extracted by projection from the solution obtained over SD-2. The conditions imposed at the lateral and downstream boundaries are the same as those used for SD-2.

The computations were carried out on a CRAY T3E-1200. Figure 6 shows the spanwise component of the vorticity at the centered horizontal plane. Figure 7 shows the side view of the elevation plot for the spanwise component of the vorticity for SD-2 and SD-3. The color indicates the value of the vorticity. SD-2 captures the Karman vortex street in the near wake and the transition, near the outflow boundary, from the first to the second phase of the vortex shedding. SD-3 successfully captures the second phase. The spacing between the vortices in the second phase is approximately twice as large compared to the spacing we see in the first phase. Near the outflow boundary of SD-2, in the transition from the first phase to the second, the vorticity loses some of its periodicity. In the upstream regions of SD-3 the vorticity shows wider peaks. Downstream, this changes to periodic sharp peaks.

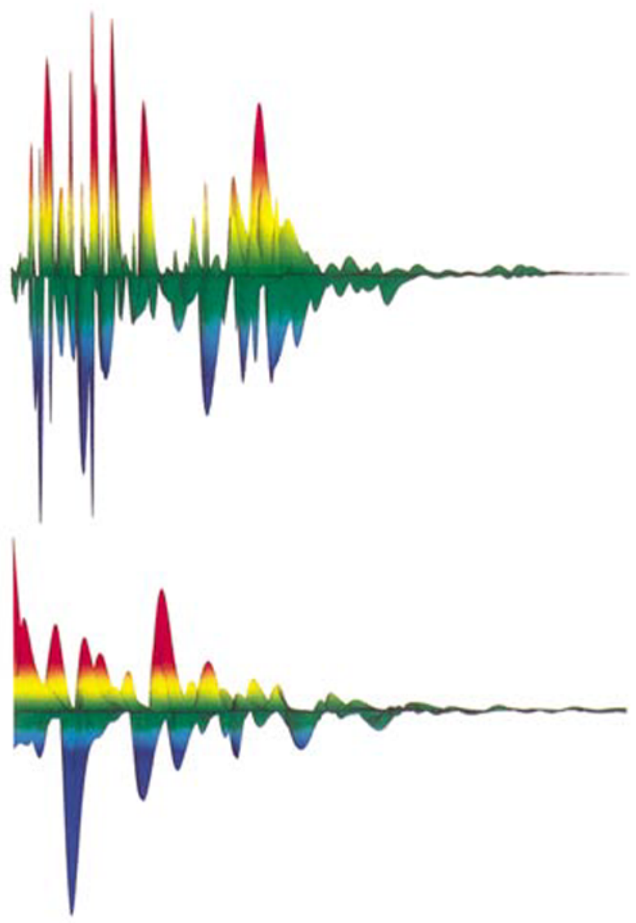

Fig. 8. 3D computation at $Re$=140. Side view of the elevation plot for the streamwise component of the vorticity at the centered horizontal plane for SD-2 (upper) and SD-3 (with different scale) (lower). The color indicates the value of the vorticity (red: positive, blue: negative).

Figure 8 shows, for SD-2 and SD-3, the side view of the elevation plot for the streamwise component of the vorticity at the centered horizontal plane. These results show us the presence of in-plane vortices for Reynolds numbers as small as 140. Although the magnitude of these vortices is much smaller compared to the spanwise vortices, the 3D behavior is evident. Comparison of 2D and 3D computations suggests that the in-plane vortices play an important role in precipitating, in far downstream, the second phase of the vortex shedding. In other words, the second phase of the vortex shedding is generated by very small 3D effects, which of course cannot be represented in a 2D simulation. We also note here that in the 2D computations we used a mesh which had more than four times as many elements compared to the in-plane mesh of the 3D computations. Despite that the 2D solution failed to capture the second phase of the vortex shedding.

# 5. Concluding Remarks

With accurate formulations and sufficiently-refined meshes, combined with the effectiveness of the Multi-Domain Method (MDM) we developed recently, we were able to simulate and visualize the details of unsteady wake flow behind a circular cylinder. We simulated and visualized two different cases. At Reynolds number 300, we showed how the MDM enables us to use highly-refined meshes and represent wake patterns which we otherwise cannot fully represent. At Reynolds number 140, we carried out the computations in both 2D and 3D. We showed that with the MDM we can extend our 3D computations sufficiently downstream, have sufficient accuracy, and capture the second phase of the Karman vortex shedding which has double the spacing between the vortices compared to the first phase. This second phase has been observed in laboratory experiments. Our computations also suggest that the transition to the second phase is caused by 3D effects.

## Acknowledgments

The work reported in this paper was partially sponsored by NASA JSC (grant no. NAG9-1059), AFOSR (contract no. F49620-98-1-0214), and by the AHPCRC under the auspices of the Department of the Army, ARL cooperative agreement no. DAAH04-95-2-0003 and contract no. DAHH04-95-0008. The content does not necessarily reflect the position or the policy of the government, and no official endorsement should be inferred. The first author has been supported by the Bridgestone Corp.

## References

[1] S. Taneda, "Downstream development of the wakes behind cylinder," Journal of the Physical Society of Japan, 14 (1959), 843-848.
[2] T. Matsui and M. Okude, "Formation of the secondary vortex street in the wake of a circular cylinder," in Structure of Complex Turbulent Shear Flow, (1983), 156-164.
[3] J. M. Cimbala, H. M. Nagib, and A. Roshko, "Large structure in the far wakes of two-dimensional bluff bodies," Journal of Fluid Mechanics, 190 (1988), 265-298.
[4] O. Inoue, T. Yamazaki, and T. Bisaka, "Numerical simulation of forced wakes around a cylinder," International Journal of Heat and Fluid Flow, 16 (1995), 327-332.
[5] C.H.K. Williamson, "Vortex dynamics in the cylinder wake," Annual Review of Fluid Mechanics, 28 (1996), 477-539.
[6] V. Kalro and T. E. Tezduyar, "Parallel 3D computation of unsteady flows around circular cylinder," Parallel Computing, 23 (1997), 1235-1248.
[7] Y. Osawa, V. Kalro, and T. E. Tezduyar, "Multi-domain parallel computation of wake flows around secondary objects," in Proceedings of the Fourth Japan-US Symposium on Finite Element Methods in Large-Scale Computational Fluid Dynamics, (1998).
[8] Y. Osawa, V. Kalro, and T. E. Tezduyar, "Multi-domain parallel computation of wake flows," Computer Methods in Applied Mechanics and Engineering, 174 (1999), 371-391.
[9] Y. Osawa and T. E. Tezduyar, "A multi-domain method for 3D computation of wake flow behind a circular cylinder," Computational Fluid Dynamics Journal, 8 (1999), 296-308.
[10] A. N. Brooks and T. J. R. Hughes, "Streamline upwind/Petrov-Galerkin formulations for convection dominated flows with particular emphasis on the incompressible Navier-Stokes equations," Computer Methods in Applied Mechanics and Engineering, 32 (1982), 199-259.
[11] T. E. Tezduyar, "Stabilized finite element formulations for incompressible flow computations," Advances in Applied Mechanics, 28 (1991), 1-44.

## *Authors' Profiles*

Yasuo Osawa: He received his M.S. from Tokyo Institute of Technology in 1988, and his Ph.D. from University of Minnesota in 1999. He is a visiting scholar at Rice University, and a staff engineer at Bridgestone Corp.

Tayfun Tezduyar: He received his Ph.D. from Caltech in 1982. He joined University of Houston as Assistant Professor in 1983 and University of Minnesota as Associate Professor in 1987. At Minnesota he was promoted to Professor in 1991 and was named a Distinguished McKnight University Professor in 1997. He was the Director of the Army HPC Research Center during the period 1994-1998. In July 1998 he was named the James F. Barbour Professor in Engineering at Rice University, and has been the Chairman of Mechanical Engineering and Materials Science since 1999. He holds a 1986 Presidential Young Investigator Award and was elected as a Fellow of the ASME in 1994. He received the 1997 Computational Mechanics Award of the Japan Society of Mechanical Engineers, the 1997 Computational Fluid Dynamics Award of the US Association of Computational Mechanics, and the 1998 Computational Mechanics Award of the International Association of Computational Mechanics.